Chinese Chemical Letters 36 (2025) 110798

Contents lists available at ScienceDirect

Chinese Chemical Letters

journal homepage: www.elsevier.com/locate/cclet

Silica coating of quantum dots and their applications in optoelectronic fields

Siting Cai[a], Xiang Chen[a], Shuli Wang[a,*], Xinqin Liao[a,c,*], Zhong Chen[a,b,c], Yue Lin[a,c,*]

[a] Fujian Engineering Research Center for Solid-State Lighting, Department of Electronic Science, School of Electronic Science and Engineering, Xiamen University, Xiamen 361005, China
[b] State Key Laboratory of Physical Chemistry of Solid Surface, Xiamen University, Xiamen 361005, China
[c] Innovation Laboratory for Sciences and Technologies of Energy Materials of Fujian Province (IKKEM), Xiamen 361102, China

ARTICLE INFO

Article history:
Received 10 November 2024
Revised 20 December 2024
Accepted 23 December 2024
Available online 26 December 2024

Keywords:
Silica-coating
Quantum dots
Light-emitting diodes
Solar cells
Photodetector

ABSTRACT

Quantum dots (QDs), a type of nanoscale semiconductor material with unique optical and electrical properties like adjustable emission and high photoluminescence quantum yields, are suitable for applications in optoelectronics. However, QDs are typically degraded under humid and high-temperature circumstances, greatly limiting their practical value. Coating the QD surface with an inorganic silica layer is a feasible method for improving stability and endurance in a variety of applications. This paper comprehensively reviews silica coating methodologies on QD surfaces and explores their applications in optoelectronic domains. Firstly, the paper provides mainstream silica coating approaches, which can be divided into two categories: *in-situ* hydrolysis of silylating reagents on QD surfaces and template techniques for encapsulation QDs. Subsequently, the recent applications of the silica-coated QDs on optoelectronic fields including light-emitting diodes, solar cells, photodetectors were discussed. Finally, it reviews recent advances in silica-coated QD technology and prospects for future applications.

1. Introduction

Quantum dots (QDs) are semiconductor nanocrystals (NCs) consisting of hundreds to thousands of atoms, with sizes ranging from a few to tens of nanometers. Their size is typically less than twice the Bohr radius of the corresponding exciton, exhibiting size-dependent quantum confinement effects [1,2]. This property allows the modification of QDs' energy band structure, resulting in distinct physicochemical characteristics and emission spectra covering the entire visible light spectrum. Based on chemical composition, QDs are categorized into four groups: Group II-VI (*e.g.*, CdSe) [3,4], Group IV-VI (*e.g.*, PbSe, PbS) [5,6], Group III-V (*e.g.*, InP) [7,8], and perovskite QDs (ABX_3 structure, where A and B are cations, X is a halide anion) [9,10]. QDs offer advantages like tunable photoemission, narrow spectra, and high photoluminescence quantum yields (PLQY), finding applications in photovoltaics [11–13], light-emitting diodes (LEDs) [14], photodetectors [15], transistors [16,17], biological monitoring [18], medical imaging [19], drug delivery [20], diagnosis [21], and treatment [22].

Despite their promising potential, QDs face challenges in practical applications due to chemical reactivity. Exposure to oxygen and moisture can cause surface degradation, leading to defect accumulation, which reduces luminescence and affects performance and stability [23]. Aggregation due to surface ligand mismatches and high concentrations further reduces quantum efficiency, increases non-radiative recombination, and weakens radiative recombination, causing color shifts. Additionally, aggregation creates large domains between QDs, impairing heat dissipation, and compromising stability. Addressing these issues is crucial for realizing the full potential of QDs in practical applications.

Here are common strategies to improve the surface instability of QDs. (i) Ion doping [24]: Introducing impurity ions like Mn^{2+}, Br^-, or I^- to modify the luminescence peak and enhance stability and efficiency. (ii) Organic ligand modification [25]: Replacing long-chain ligands such as oleic acid (OA) with alternatives (*e.g.*, lecithin, dodecanethiol, *N′*-(2-aminoethyl)-*N′*-hexadecylethane-1,2-diamine, vinyl phosphonic acid, octylphosphonic acid, dimethyldidodecylammonium bromide) [26–31] to reduce non-radiative decay and improve QD performance and stability. (iii) Polymer encapsulation [32–34]: Using polymers (*e.g.*, polystyrene (PS), polyvinyl alcohol, polydimethylsiloxane) to shield QDs from oxygen and moisture, increasing their stability. (iv) Inorganic encapsulation [35]: Coating QDs with inorganic compounds like ZnS, ZnO, or SiO_2

* Corresponding authors.
E-mail addresses: slwang@xmu.edu.cn (S. Wang), liaoxinqin@xmu.edu.cn (X. Liao), yue.lin@xmu.edu.cn (Y. Lin).

https://doi.org/10.1016/j.cclet.2024.110798
1001-8417/

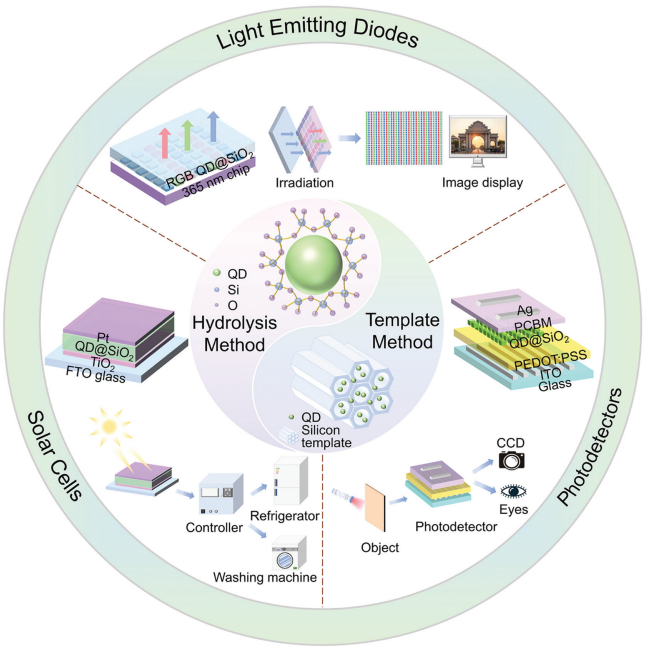

Fig. 1. The approaches of silica coating on QD surfaces (inner circle) and their applications in optoelectronic fields (outer circle).

to provide a rigid protective layer, with silica being particularly effective due to its optical stability, chemical resistance, and biocompatibility. Among the inorganic encapsulation compounds, silica stands out as an ideal material for coating QDs, due to the exceptional optical, chemical stability, and biocompatibility. Apart from the enhanced performance of QDs, the moderate refractive index and excellent light transparency of silica make it suitable for adjusting the performance of QDs-based optical devices. *In-situ* hydrolysis of siliconizing reagent on the QDs surfaces and encapsulation of QDs in silica template are two mainstream approaches to achieve effective silica coating on QDs (Fig. 1, inner circle). By adjusting the coating method and the operating conditions, the thickness and uniformity of the silicon dioxide coating layer on the surface of QDs can be precisely controlled to meet different application scenarios (Fig. 1, outer circle).

In this paper, we review the silica coating methods on QD surfaces and their applications in optoelectronic fields. Firstly, we introduced the silica coating approaches, which can be classified into *in-situ* hydrolysis of silylating reagents on QD surfaces and encapsulation of QD in silica template, according to the coating mechanism. Next, we discuss the applications of silica-coated QDs in the optoelectronic field, focusing on their use in LEDs, solar cells, and photodetectors. Finally, we provide a comprehensive overview of the review and offer a forward-looking analysis of emerging trends, potential challenges, and future prospects in this domain.

2. Coating methods of silica on QDs

Researchers developed various technical approaches to produce the silica-coated QDs. Based on the coating mechanism, these approaches can be classified into *in-situ* hydrolysis of silylating reagents on QD surfaces and encapsulation of QD in silica template. The first method involves the hydrolysis of silane coupling agent in QD dispensed solvent for *in-situ* formation of silica coating on the surfaces of the pre-synthesized QDs. The second method refers to the synthesis of QDs in a porous matrix primarily composed of silica and encapsulating them within it. In the subsequent sections, these two approaches will be comprehensively introduced.

2.1. In-situ hydrolysis of silylating reagents on QD surfaces

Hydrolysis is a common chemical synthesis technique used for creating thin films and nanomaterials, often involving silicon precursors like ethyl orthosilicate (TEOS), methyl orthosilicate (TMOS) and aminopropyl triethoxysilane (APTES), which form silanols and polymerize into siloxane networks [36]. Taking TEOS as an example, it reacts with water to form a silica coating on QDs. Hydrolysis involves hydroxyl groups (OH^-) displacing ethoxy groups (OC_2H_5) from TEOS, producing silanol and ethanol (Eq. 1). The silanol further reacts with water to generate more silanol (Eqs. 2-4), which then condenses into a silica network through silicon-oxygen bonds (Si-O-Si) (Eq. 5) [37]. The choice of silicifiers depends on material properties required for specific applications. For example, APTES provides more surface functionalization due to its amino groups. Currently, silica-coated QDs are prepared mainly through sol-gel and reverse microemulsion techniques. Below, we will discuss the advancements in these methods for preparing silica-coated QDs.

$$Si(OC_2H_5)_4 + 4H_2O \rightarrow 4Si(OH)(OC_2H_5)_3 + 4C_2H_5OH \quad (1)$$

$$Si(OH)(OC_2H_5)_3 + H_2O \rightarrow Si(OH)_2(OC_2H_5)_2 + C_2H_5OH \quad (2)$$

$$Si(OH)_2(OC_2H_5)_2 + H_2O \rightarrow Si(OH)_3(OC_2H_5) + C_2H_5OH \quad (3)$$

$$Si(OH)_3(OC_2H_5) + H_2O \rightarrow Si(OH)_4 + C_2H_5OH \quad (4)$$

$$2Si(OH)_4 \rightarrow (OH)_3Si\text{-}O\text{-}Si(OH)_3 + H_2O \quad (5)$$

2.1.1. Sol-gel method

The sol-gel method is a material synthesis methodology that is commonly used to create coatings or films of metal oxides and other inorganic substances [38]. First, QDs are synthesized using methods such as thermal injection and ligand-assisted reprecipitation. Then, silicification reagents, such as TEOS or TMOS, are introduced into organic solvents containing QDs. An appropriate amount of water is added to promote the hydrolysis and condensation reactions of the silanization reagents on the surface of the QDs, ultimately forming a silica matrix.

Liu *et al.* encapsulated $CsPbBr_3$@glass with a hydrophobic silica layer using the sol-gel method (Fig. 2A(i)) [39]. This was achieved through the ozonolysis reaction between tri-(dimethylamine)silane and O_3, which formed a dense silica layer ($CsPbBr_3$@Glass@A). Dibutyltin diformate was then used to catalyze the polymerization of TEOS and polydimethylsiloxane, creating a hydrophobic silica network ($CsPbBr_3$@glass@ASG). The dense silica layer had an average thickness of 29.0 ± 3.4 nm, while the hydrophobic layer was 40.1 ± 7.7 nm thick. This structure improved water resistance, thermal reversibility of PL, and light stability. After 7 weeks, $CsPbBr_3$@glass@ASG retained 100% of its PL intensity and 88% of its light intensity, while $CsPbBr_3$@Glass@A kept 90% PL and 81% light intensity. In contrast, uncoated $CsPbBr_3$@glass retained only 60% of its PL intensity and 50% of its light intensity (Fig. 2A(ii, iii)). Thus, $CsPbBr_3$@Glass@ASG balances optical properties and external stability.

Ding *et al.* synthesized silica-coated ZnO QDs (ZnO@SiO_2) using an advanced sol-gel method and prepared a QD-composite ink by combining ZnO@SiO_2 with polyvinyl alcohol for UV-protective coatings on PET films [40]. The silica coating significantly reduced the photocatalytic activity of QDs, preventing the degradation of Rhodamine B and avoiding ZnO QD aggregation in water. UV–vis

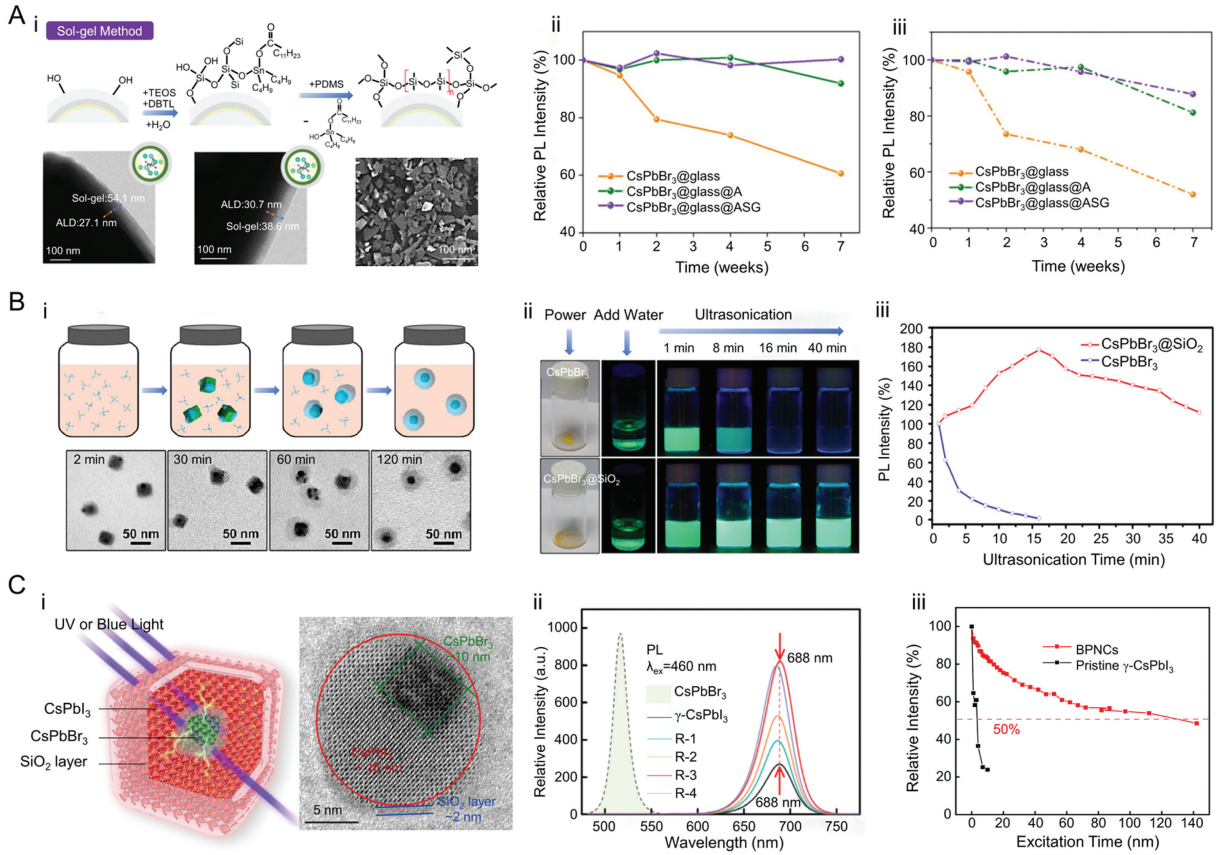

Fig. 2. Synthesis of silicon-coated QDs by sol-gel method. (A): (i) The mechanism of synthesizing SiO_2 coating by sol-gel method (on top), and high-resolution transmission electron microscope (HRTEM) of $CsPbBr_3$@glass@ASG (on bottom), (ii) The PL intensity and (iii) the optical density of different samples during waterproof testing. Reproduced with permission [39]. Copyright 2023, John Wiley & Sons. (B): (i) The formation of $CsPbBr_3@SiO_2$ (on top), and transmission electron microscope (TEM) images of QD with different reaction times (on bottom); (ii) Water stability test for $CsPbBr_3$ NCs and $CsPbBr_3@SiO_2$; (iii) The PL intensity of QDs in aqueous solutions following various ultrasonication durations. Reproduced with permission [41]. Copyright 2018, American Chemical Society. (C): (i) The structure (left), and HRTEM of BPNC (right); (ii) PL spectra of different samples; (iii) Light absorption of BPNC and pristine γ-$CsPbI_3$ PQDs under continuous excitation with blue LEDs. Reproduced with permission [44]. Copyright 2023, John Wiley & Sons.

transmission spectra of the QD-composite ink coatings showed excellent UV-blocking capabilities below 355 nm while maintaining high transparency in the visible range. After 100 h of exposure to 30 W UV light, the coatings' UV–vis spectra remained largely unchanged, demonstrating the long-term durability of the QD-based composite materials.

Though the sol-gel method can produce silica coating on QDs by hydrolysis of siliconizing reagent, most of the silica-coated particles contain several QD nanoparticles and possess a relatively large dimension, which makes these silica-coated QDs unsuitable for applications that require high precision, such as QD-based color conversion micro-LED displays. Therefore, obtaining single QD particles coated with silicon dioxide is crucial for the construction of some advanced QD-based devices.

Zhong *et al.* synthesized monodispersed core-shell $CsPbBr_3@SiO_2$ by controlling the hydrolysis reaction time [41]. $CsPbBr_3$ QDs were formed by rapidly injecting toluene into a DMF solution of CsBr, $PbBr_2$, and ligands OA and Oleylamine (OAm). The pH was adjusted with ammonia, and rapid injection into toluene precipitated $CsPbBr_3$ QDs. The mixture was then added to super-dried toluene with TMOS, where hydrolysis produced silica oligomers that adsorbed onto the QD surfaces. Continued hydrolysis and condensation encapsulated $CsPbBr_3$ QDs in a silica shell (Fig. 2B(i)). After 2 min, the NCs retained their cubic structure, but extending hydrolysis to 60 min increased silica thickness to about 14 nm, rising to 17 nm at 120 min. Uncoated $CsPbBr_3$ QDs lost PL after 16 min of ultrasonication, while $CsPbBr_3@SiO_2$ QDs maintained bright emission for 40 min, showing enhanced stability (Fig. 2B(ii)). The PL intensity of uncoated QDs dropped to 0% after 16 min, whereas $CsPbBr_3@SiO_2$ QDs showed higher water dispersibility and PL intensity (177%) after ultrasonication, with a slight decrease to 112% after extended exposure. The silica shell significantly improved the stability of $CsPbBr_3@SiO_2$ QDs by protecting the core from water-induced degradation (Fig. 2B(iii)).

Meng *et al.* used APTES as a bifunctional surface ligand to passivate $CsPbBr_3$ QDs' surface defects and form Si-O-Si covalent bonds *via* -$SiOCH_3$ and -SiOH groups [42]. This dual functionality enhanced the surface chemistry of the perovskite QDs. By carefully controlling the silane hydrolysis rate, the authors synthesized $CsPbBr_3@SiO_2$ QDs with a uniform silica shell thickness ranging from 1 nm to 2.7 nm, preserving their original cubic shape and optical properties. Complete silica encapsulation significantly boosted the QDs' robustness, maintaining 90% of their initial PL intensity after 6 h in high-humidity conditions.

Compared to green-emissive $CsPbBr_3$ QDs, red-emissive $CsPbI_{3-x}Br_x$ perovskite QDs exhibit poorer PL and stability due to higher trap density and ion migration in harsh environments. Chao *et al.* successfully coated both $CsPbBr_3$ and $CsPbI_{3-x}Br_x$ perovskite QDs ($CsPbBr_3@SiO_2$ and $CsPbI_{3-x}Br_x@SiO_2$) using a sol-gel method [43]. After synthesizing the QDs, silane coupling agents were added to the solution, initiating a silanization reaction at room temperature. This protective silica layer significantly improved the QDs' stability, resulting in $CsPbX_3@SiO_2$ QDs with

narrow emission peaks in their PL spectra, indicating enhanced optical properties.

Fan *et al*. developed a bicomponent perovskite nanocomposite (BPNC) material, which consists of $CsPbBr_3$ QDs (green light) at the core, γ-$CsPbI_3$ QDs (red light) at the shell, encapsulated by a silica layer both in the interlayer and as the outermost layer (Fig. 2C(i)) [44]. This structure facilitates energy transfer from the core to the shell *via* a non-radiative fluorescence resonance energy transfer process, enhancing red luminescence intensity (Fig. 2C(ii)). Under blue light excitation, the PL intensity increases over threefold, with the PLQY nearing 100%. The silica layer is crucial, and it acts as a barrier to prevent diffusion between the core and shell, preserving their structural integrity. Additionally, the outer silica coating protects the QDs and enhances BPNC stability. Even under continuous blue light excitation (5 V, 10 mA), BPNCs exhibit significantly improved blue light tolerance, with a half-life of about 2 h, outperforming original γ-$CsPbI_3$ in stability (Fig. 2C(iii)). These results demonstrate that the coating structure provides good stability for BPNC.

2.1.2. Reverse microemulsion method

The reverse microemulsion method synthesizes QD samples with specific sizes and shapes using tiny oil-in-water (O/W) or water-in-oil (W/O) type emulsion droplets as reaction vessels [45]. Initially, QDs are synthesized *via* heat injection or ligand-assisted reprecipitation and serve as the core for subsequent coating. The QDs are then dispersed in an inverse microemulsion containing a surfactant (*e.g.*, IGEPAL CO-520), a hydrophobic solvent (like *n*-hexane or octane), and water, ensuring each QD is surrounded by microemulsion droplets. Introducing silicon dioxide precursors (*e.g.*, TEOS, TMOS) leads to hydrolysis and condensation within these droplets, forming a silicon dioxide coating on the QDs' surfaces.

An *et al*. employed the microemulsion method to coat silica on CdSe/ZnS QDs [46]. By adding ammonia water to a cyclohexane solution of IGEPAL CO-520 and TEOS, a stable interface between water and oil is created, forming a microemulsion. Ammonia water catalyzes TEOS reaction, leading to silica growth on the QDs. By varying TEOS amounts and reaction times, they produced QDs@SiO_2 with shell thicknesses from 11 nm to 56 nm. The CdSe/ZnS QDs exhibited an absorption peak at 612 nm and an emission peak at 626 nm, with a FWHM of 24 nm. Notably, increasing the silica shell thickness did not change the emission peak, though the FWHM of QDs@SiO_2 nanoparticles slightly widened to 26 nm.

Lv *et al*. successfully engineered hydrophobic CdSe/ZnS QDs with a biocompatible silica coating using a novel reverse microemulsion method [47]. The resulting QDs have a narrow size distribution, averaging about 14 nm in diameter, and the silica-coated QDs maintain a uniform size distribution with an average diameter of 29 nm. Remarkably, the PL intensity of these QDs remains stable across varying temperatures, with almost 100% intensity from 20 °C to 50 °C and 80% at 90 °C. Additionally, after 12 h under a 365 nm UV lamp, the PL intensity of the silica-encapsulated QD solution remains at 85% of its initial value.

Tang *et al*. prepared ultra-thin, core-shell structured silica-coated Mn^{2+}-doped $CsPbX_3$ (X = Br, Cl) QDs using a simple reverse microemulsion method [48]. The process started with a DMF precursor solution of $PbBr_2$, $PbCl_2$, $MnBr_2$, and CsBr introduced into toluene at room temperature, followed by the addition of TEOS as a silane source. After TEOS hydrolysis, a silica layer was deposited on the QDs, forming orthorhombic $CsPbMnX_3$ QDs. To reduce the hydrolysis reaction of TEOS, trioctylphosphine oxide (TOPO) is selected as a surfactant to modify the surface of QDs, which can effectively prevent the cleavage of $CsPbMnX_3$ core QDs caused by silane hydrolysis (Fig. 3A). Each QD was encased in a silica shell, indicating isotropic growth and a smooth surface (Fig. 3B). During water resistance testing, uncoated $CsPbMnX_3$ QDs lost luminescence after 6 days, while the silica-coated QDs maintained approximately 90% of their initial efficiency in aqueous media (Figs. 3C and D).

Huang *et al*. combined reverse microemulsion with surface modification to synthesize ZnO@SiO_2 QDs with a core-shell structure and transparent nanodispersions [49]. These ZnO@SiO_2 QDs, with a thick silica shell and an average diameter of 12 nm, exhibited excellent monodispersity in toluene, high optical transparency, and significant UV absorbance, making them suitable for UV protection and optoelectronic applications. The highly transparent ethyl cellulose/ZnO@SiO_2 composite film remained optically stable after 100 h of UV aging due to the dispersion's properties.

2.2. Template method for encapsulation QDs

The template method is a versatile and effective technique for fabricating nanomaterials with customized shapes and sizes, particularly in the synthesis of silica-coated QDs [50]. Typically, mesoporous silica materials like molecular sieves are used as templates. These templates are immersed in a solution containing QD precursors, allowing the precursor molecules to penetrate the pores, where they undergo chemical reactions to form QDs. To enhance the crystallization and growth of QDs within the silica matrix, heat treatment is often necessary. This synthesis can be divided into two strategies based on temperature: the low-temperature synthesis method and the high-temperature solid-state method, each designed to achieve precise control and optimize the performance of the QDs.

2.2.1. Low-temperature synthesis

The low-temperature synthesis method utilizes silica molecular sieves as templates to grow QDs inside them at low temperatures. The growth speed of QDs in the template is relatively slow, which makes the size and shape of the QDs accurately controllable, and a uniform thickness of silica coating.

Fan *et al*. encapsulated $CsPbBr_3$ in mesoporous silica SBA-15, which has a large surface area, uniform pores, high refractive index, and is stable up to 120 °C [51]. Perovskite QDs were synthesized *in situ* within the pores by mixing PbO, phenacyl bromide, and SBA-15 in 1-octadecene under nitrogen. After adding a cesium source, QDs formed and diffused into the SBA-15 (Fig. 4A(i)). The 10.5 nm pore size of SBA-15 accommodated 8.6 nm $CsPbBr_3$ QDs, enhancing their PLQY from 24.84% to 63.96% and luminescence lifetime from 32.6 ns to 104.97 ns (Fig. 4A(ii, iii)). The SBA-15′s ordered structure reduces ion diffusion, improves crystallinity, and passivates surface defects, preserving 95% of the QDs' initial PL after six months, compared to 55% for pure $CsPbBr_3$, showing the material's superior stability against water and oxygen (Fig. 4A(iv)).

Huang *et al*. synthesized mesoporous silica (m-SiO_2) using Pluronic F108, hydrochloric acid (HCl), trimethylphenol (TMB), and TEOS [52]. $CsPbBr_3$ QDs were then produced at 110–160 °C within the hollow mesoporous structure. The silica structure contained silanol sites that adsorbed cesium and bromine ions, forming $CsPb_2Br_5$ impurities detrimental to QD performance ($CsPbBr_3$@SiO_2 OH). To address this, the authors treated the structure with trimethylchlorosilane (TMCS) to eliminate silanol groups, preventing impurity formation and yielding a purer $CsPbBr_3$@SiO_2 TMe (Fig. 4B(i)). After synthesis, perovskite QDs were dispersed in the hollow mesoporous silica. The crystal plane spacing of $CsPbBr_3$@SiO_2 TMe is 0.341 nm, corresponding to the (111) plane of orthorhombic $CsPbBr_3$, whereas $CsPbBr_3$@SiO_2 OH showed spacings of 0.410 nm and 0.217 nm, related to $CsPb_2Br_5$ (Fig. 4B(ii)). Under 80% humidity at 28 °C, $CsPbBr_3$@SiO_2 TMe retained 87% of its PL intensity after 720 h, while $CsPbBr_3$@SiO_2 OH dropped to 10%

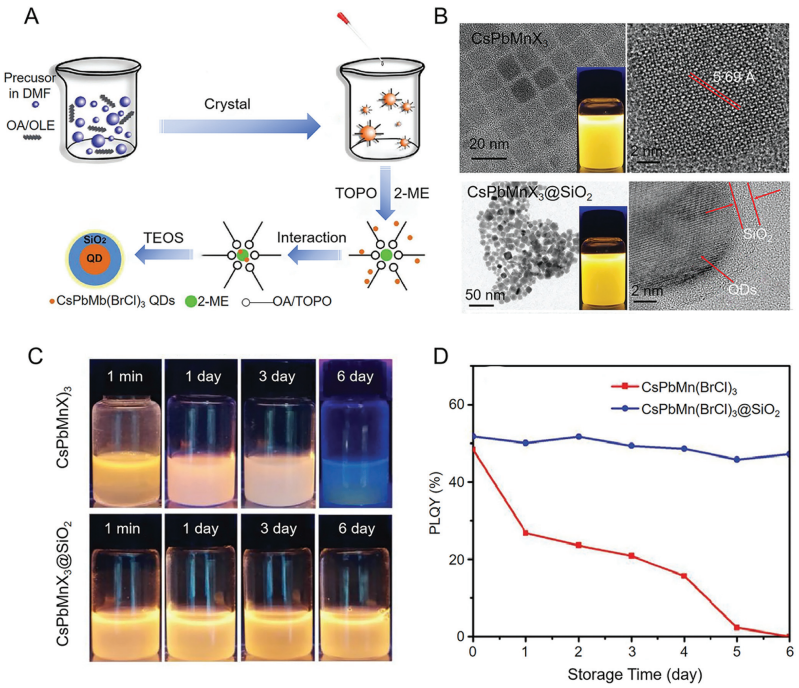

Fig. 3. Synthesis of silica-coated QDs by reverse microemulsion method. (A) Schematic diagram of the process of synthesizing $CsPbMnX_3@SiO_2$ core-shell QDs. (B) TEM and HRTEM images of $CsPbMnX_3$ QDs and $CsPbMnX_3@SiO_2$. (C) Images of $CsPbMnX_3$ and $CsPbMnX_3@SiO_2$ QDs in aqueous solution under ultraviolet light. (D) PLQY of $CsPbMnX_3$ and $CsPbMnX_3@SiO_2$ QDs. Reproduced with permission [48]. Copyright 2019, John Wiley & Sons.

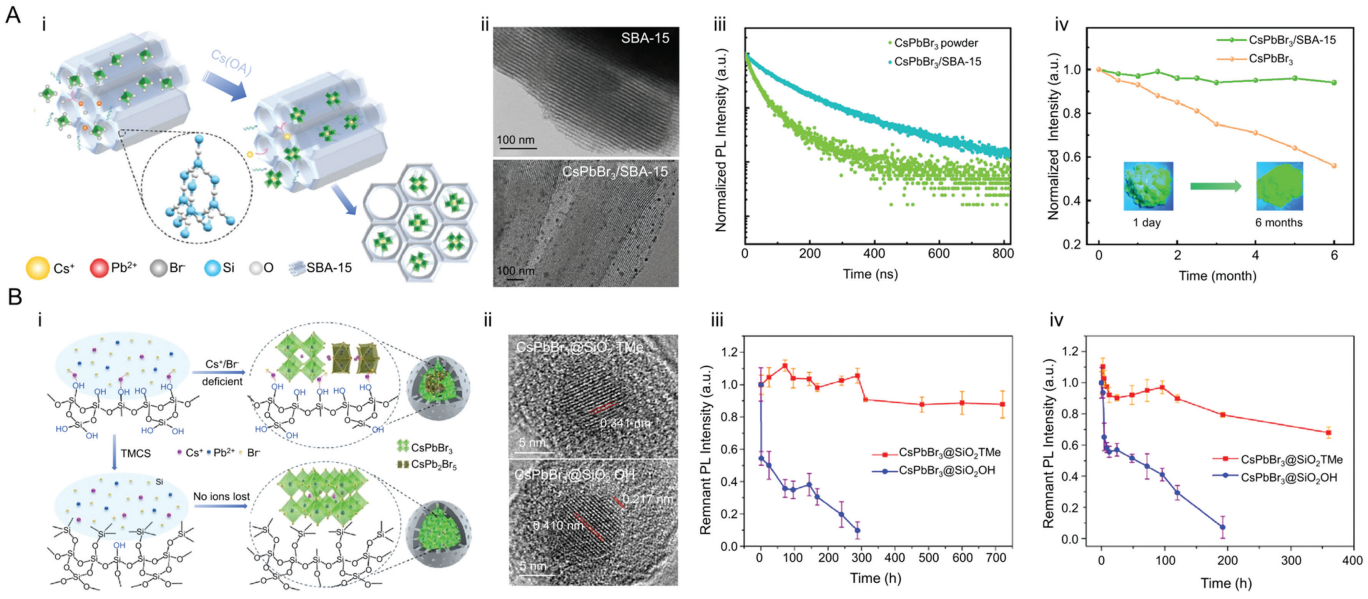

Fig. 4. Low-temperature synthesis of silica-coated QDs. (A): (i) Synthesis diagram of $CsPbBr_3$/SBA-15; (ii) TEM image of SBA-15 and $CsPbBr_3$/SBA-15; (iii) Time-resolved PL decays of $CsPbBr_3$ and $CsPbBr_3$/SBA-15; (iv) PL stability of $CsPbBr_3$ and $CsPbBr_3$/SBA-15 at room temperature. Reproduced with permission [51]. Copyright 2023, John Wiley & Sons. (B): (i) Synthesis diagram of $CsPbBr_3@SiO_2$ OH and $CsPbBr_3@SiO_2$ TMe; (ii) TEM images of $CsPbBr_3@SiO_2$ TMe and HTEM images of $CsPbBr_3$@h-SiO_2 OH; (iii) Moisture stability of $CsPbBr_3@SiO_2$ OH and $CsPbBr_3@SiO_2$ TMe; (iv) Thermal stability of $CsPbBr_3@SiO_2$ OH and $CsPbBr_3@SiO_2$ TMe. Reproduced with permission [52]. Copyright 2023, John Wiley & Sons.

after 288 h. Similarly, after 360 h, $CsPbBr_3@SiO_2$ TMe maintained 68% of its PL intensity, whereas $CsPbBr_3@SiO_2$ OH retained only 7% after 192 h, indicating superior stability of $CsPbBr_3@SiO_2$ TMe (Fig. 4B(iii, iv)).

Chen *et al.* utilized ordered mesoporous silica (m-SiO_2) as a microreactor for *in-situ* growth of ultra-small $CsPbBr_3$ QDs at environmental factors. The PLQY of the resulting $CsPbBr_3$/m-SiO_2 (CPB/MS) powder reached 68%, significantly higher than the 180 °C [53]. This method suppressed excessive QD growth, light, the luminescence decay of CPB/MS nanocomposites was value, compared to 16% for discrete $CsPbBr_3$ powder. Thus, the CPB/MS material showed remarkable chemical stability, enhanced resistance to luminescence decay, and superior thermal quenching performance.

2.2.2. High-temperature solid-state synthesis

Compared with low-temperature synthesis, high-temperature conditions improve the control of QD size and morphology due to accelerated reaction rates, allowing precursor molecules to react and deposit uniformly in silica microspheres. This enhances production efficiency and is suitable for large-scale production. Cru-

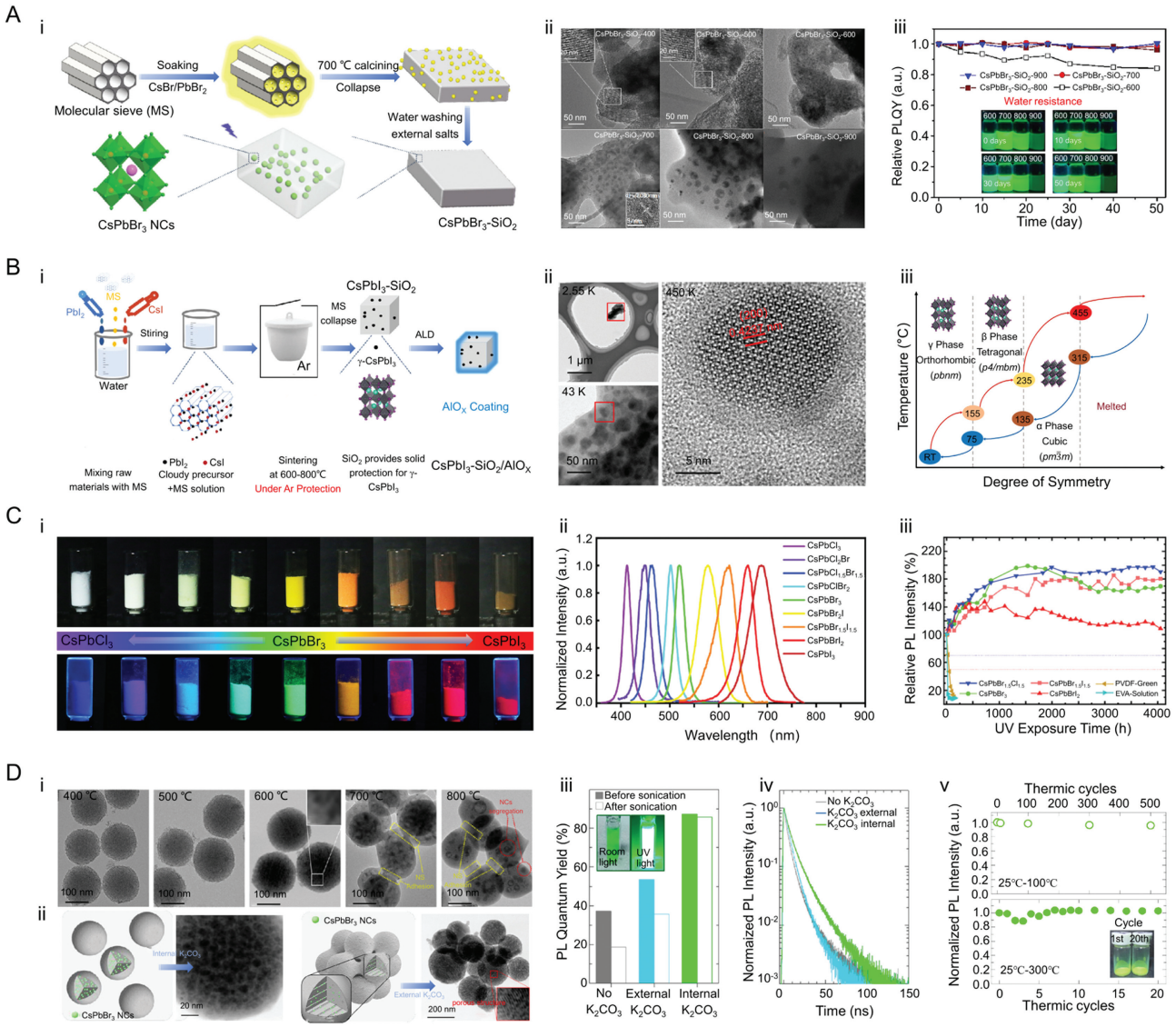

Fig. 5. High-temperature solid-state synthesis of silica-coated QD. (A): (i) The schematic diagram for the synthesis of $CsPbBr_3$-SiO_2; (ii) TEM images of $CsPbBr_3$-SiO_2 at different calcination temperatures; (iii) The PLQY of $CsPbBr_3$-SiO_2 synthesized at different calcination temperatures in water immersion. Reproduced with permission [54]. Copyright 2020, Springer Nature. (B): (i) The schematic diagram of synthesis $CsPbBr_3$-SiO_2; (ii) TEM images of $CsPbI_3$-SiO_2 with different magnifications; (iii) The phase transition routes of $CsPbI_3$-SiO_2. Reproduced with permission [55]. Copyright 2021, John Wiley & Sons. (C): (i) Image of the PeNCs-SiO_2 family exposed to UV light at 365 nm and daylight; (ii) PL spectra of the PeNCs-SiO_2 family; (iii) PL intensity in UV light conditions changes. Reproduced with permission [56]. Copyright 2021, Royal Society of Chemistry. (D): (i) TEM images of $CsPbBr_3$-SiO_2 NCs at different calcination temperatures; (ii) Schematic and TEM images of $CsPbBr_3$-SiO_2 NCs obtained by internal sintering and external sintering of K_2CO_3 at 600 °C, respectively; (iii) PLQY of ultrasound in water; (iv) PL decay traces of the samples; (v) Normalized PL strength of internal K_2CO_3 sintered $CsPbBr_3$-SiO_2 NCs collected during 25-100 °C heat treatment (top) and 25-300 °C annealing (bottom) in air. Reproduced with permission [58]. Copyright 2022, American Chemical Society.

cially, the mesoscopic structure of porous SiO_2 is compromised when merged in melted precursor salt at high temperatures, resulting in a solidified structure that encapsulates the QDs, enhancing their robustness. Selecting appropriate silica microspheres as templates allows for precursor molecule introduction into their pores, transforming into QDs during subsequent heat treatment. The silicon source material deposits on the QDs' surfaces at high temperatures, forming a silicon coating layer.

Zhang *et al.* encapsulated $CsPbBr_3$ in a SiO_2 porous matrix using high-temperature solid-state synthesis [54]. Porous all-silicon molecular sieve templates were immersed in a precursor salt solution (CsBr and $PbBr_2$) and dried at 80 °C. The composites were then heated to 600–900 °C, leading to the formation of $CsPbBr_3$ QDs within the molecular sieve's closed pores. As the pore structure collapsed, the molecular sieve encapsulated the QDs, resulting in dense $CsPbBr_3$-SiO_2 composites (Fig. 5A(i)). At 400 °C and 500 °C, the pores remained stable, preventing collapse and delaying QD formation. However, at 600 °C, the pore structure collapsed, creating small $CsPbBr_3$ QDs. As the calcination temperature rose, the molecular sieve's pores softened, reducing the template's confinement effect, causing QD size to increase from 6.7 nm to 30.1 nm (Fig. 5A(ii)). The highest PLQY of 63% was achieved in the $CsPbBr_3$-SiO_2–700 sample ($CsPbBr_3$ to molecular sieve's mass ratio of 1:3, calcination temperature of 700 °C), while other conditions yielded PLQY below 45%. The silica-coated QDs demonstrated excellent stability; after 50 days in water, the $CsPbBr_3$-SiO_2–600 sample retained 88% of its initial PLQY. In contrast, $CsPbBr_3$-SiO_2 samples synthesized at higher temperatures (700 °C, 800 °C, and 900 °C) maintained their PLQY (Fig. 5A(iii)). The stability of the $CsPbBr_3$-SiO_2 samples in water highlighted

the effectiveness of silica coating in protecting QDs from degradation.

Lin *et al*. successfully synthesized γ-$CsPbI_3$ NCs encapsulated with SiO_2/AlO_x using high-temperature sintering and atomic layer deposition (ALD) techniques (Fig. 5B(i)) [55]. Initially, CsI and PbI_2 were mixed with MCM-41 to form a precursor solution. The solution was sintered at 700 °C under nitrogen, collapsing the MCM-41 structure into amorphous SiO_2, which trapped $CsPbI_3$ NCs. To enhance stability, an AlO_x layer was deposited using ALD, preventing oxygen penetration and oxidation. As shown in Fig. 5B(ii), $CsPbI_3$ are uniformly distributed in the SiO_2 matrix, with a spherical structure of about 20 nm and a lattice spacing of 0.42 nm corresponding to the (200) plane of $CsPbI_3$. The SiO_2/AlO_x encapsulated $CsPbI_3$ nanocrystals undergo a direct phase transition from γ to α *via* β upon heating, and reversely from α to γ through β when cooling, bypassing the δ phase (Fig. 5B(iii)). This novel phase transition is facilitated by the protective SiO_2/AlO_x encapsulation, which significantly enhances the phase stability of the $CsPbI_3$ NCs. Moreover, after 3000 h of water immersion and UV irradiation tests, minimal PL strength loss was observed, indicating excellent water and UV resistance.

Lin *et al*. extended their method to perovskite QDs with various halide components, achieving PL covering the entire visible spectrum (Fig. 5C(i, ii)) [56]. After 1560 h in ambient conditions, silica-coated QDs showed superior PL stability under UV exposure compared to polymer-coated controls (Fig. 5C(iii)). Additionally, these silica-coated QDs demonstrated improved stability in water. Yang *et al*. enhanced the stability of $CsPbBr_3$ QDs against water, light, and heat by embedding them in mesoporous silica microspheres ($CsPbBr_3$ PQDs/MSs) through high-temperature synthesis [57]. The $CsPbBr_3$ PQDs/MSs retained over 80% of their initial PL intensity after 2 weeks in water and about 90% after 6 h at 150 °C.

During high-temperature silica coating, QDs and silica tend to form large particles (Fig. 5D(i)). He *et al*. minimized this aggregation using K_2CO_3, producing silica-coated $CsPbBr_3$ QDs with a size of 8.6 ± 1.3 nm [58]. By sintering potassium carbonate inside and outside the silica, they prevented particle fusion and increased PLQY from 37% to 87% (Fig. 5D(ii, iii)). Ultrasonic treatment in water significantly reduced the PLQY of non-treated and externally sintered samples, but the internally sintered QDs maintained a PLQY of 85%, confirming the protective effect of collapsed pores. Additionally, K_2CO_3 extended the lifetimes of the sintered particles and improved thermal stability up to 300 °C (Fig. 5D(iv, v)).

Song *et al*. fabricated $CsPbX_3@SiO_2$ composites with stable PLQY values of 11.4%, 80.6%, and 16.2% for red, green, and blue QDs, respectively, over 30 days at 25 °C and 80% humidity [59]. However, the PLQY of red QDs from high-temperature synthesis remains low. Deng *et al*. improved this by incorporating Zn to passivate defects, resulting in red silica-coated $CsPbI_3$-Cs_4PbI_6 QDs with a PLQY of 43.58% and stable PL after 1100 h in water and ambient storage [60].

3. Applications of silica-coated QDs

The silica-coated can improve the performance of QDs, such as increased PL intensity, PLQY, narrowed FWHM, enhanced stability at various conditions. Currently, the applications of silica-coated QDs are mainly focused on optoelectronic applications, specifically LED, solar cells, and photodetector. In this section, we will introduce the applications of silica-coated QDs in these scenarios.

3.1. Light-emitting diodes

LEDs, semiconductor light sources that emit light through electron-hole recombination in the PN junction, are crucial in daily lighting, displays, signaling systems, medical instruments, and automotive lighting [61,62]. Silica-coated QDs serve as color-converted layers in white LEDs, backlight layers for liquid crystal displays, and as red/green/blue color pixels in micro-LED displays, usually excited by UV or blue LEDs [63]. These QDs can also function as emitting layers in QD LED (QLED) displays.

Wang *et al*. fabricated red, green, and blue $CsPbX_3@SiO_2$ NCs films for white-LED (WLED) devices, achieving PLQYs of 10.9%, 94.0%, and 33.7%, respectively, after silica coating (Fig. 6A(i, ii)) [64]. These films demonstrated enhanced stability against UV irradiation, thermal shock, and humidity. The resulting WLEDs exhibited a high CRI of 93.4, CIE coordinates of (0.327, 0.343), an NTSC color gamut of 126.4%, and a luminous efficacy of 47.75 lm/W (Fig. 6A(iii)). The spectra remained stable even after 36 h of continuous operation. Notably, $CsPbX_3@SiO_2$ NC films show scalability and bendability on flexible substrates, broadening their application potential (Fig. 6A(iv, v)).

Chen *et al*. explored silica-coated perovskite QDs ($CsPbX_3$@AGs) as backlight films [65]. When excited by gallium nitride LED, $CsPbCl_2Br$@AGs, $CsPbBr_3$@AGs, and $CsPbBrI_2$@AGs emitted bright blue, green, and red light, respectively (Fig. 6B(i)). After dispersing the silica-coated QDs in PS, $CsPbBr_3$@AGs@PS membranes emitted green light at 518 nm, while $CsPbBrI_2$@AGs@PS membranes emitted red light at 632 nm. Under blue backlighting, the composite film achieved a white light coordinate of (0.3010, 0.3108) with a red-green-blue ratio of 26.2%:68.3%:5.5%, closely resembling commercial backlight films (Fig. 6B(ii)). The $CsPbX_3$@AGs films showed performance comparable to or superior to commercial CdSe-based backlights (Fig. 6B(iii, iv)). After 48 h of continuous illumination, the luminous flux remained above 99.5% of the initial value, demonstrating excellent optical stability (Fig. 6B(v)).

For QD-based full-color micro-LED displays, QDs need to be patterned, which may weaken their performance due to chemical contact [66,67]. Silica coating protects QDs from damage during patterning, improving micro-LED display performance and stability. Chang *et al*. synthesized silica-coated CdSe/ZnS QDs and prepared QD photoresist (QDPR) for patterning *via* photolithography (Fig. 6C(i)) [68]. A patterned black matrix minimized light crosstalk, and a distributed Bragg reflector (DBR) enhanced color purity (Fig. 6C(ii)). The DBR layer, patterned red and green QDPR color conversion layer, and blue micro-LED chips were bonded to prepare the full-color micro-LED display panels, which showed a color gamut of 88.74% Rec. 2020 standard (Fig. 6C(iii)). The displays showed a brightness decay rate below 15% at 85 °C and 90% humidity after 500 h, indicating excellent stability (Fig. 6C(iv)).

In QLED devices, QDs are excited by injecting electrons and holes that recombine to emit photons. The performance of QLEDs depends on factors such as QD quality and the electron and hole injection rates [69,70]. The ligands and coatings of QDs impact carrier transfer and luminescent properties, and silica's low electric conductivity makes it generally unsuitable for QD coatings despite improving stability. Thus, adjusting the SiO_2 coating thickness is crucial for enhancing silica-coated QDs in QLED devices.

Trinh *et al*. created $CsPbBr_3@SiO_2$ as the emission layer, resulting in improved chemical and electrical stability and enhanced device performance [71]. The device structure comprised ITO/PEDOT:PSS/A-$CsPbBr_3@SiO_2$/TPBi/LiF/Al, with A-$CsPbBr_3@SiO_2$ QDs averaging 15–27 nm, larger than pure $CsPbBr_3$ (11 nm) (Fig. 7A(i)). They noted higher current density in QLEDs with uncoated $CsPbBr_3$ QDs due to pinholes, while initial brightness increased slowly, suggesting non-radiative recombination (Fig. 7A(ii)). In contrast, A-$CsPbBr_3@SiO_2$ QD-based QLEDs reached maximum brightness of 3200 cd/m² at 830 mA/cm², with current efficiency of 5.3 cd/A, indicating more effective use of electrons and holes (Fig. 7A(iii, iv)). This signifies a higher light output per unit current, indicating a more efficient utilization of both

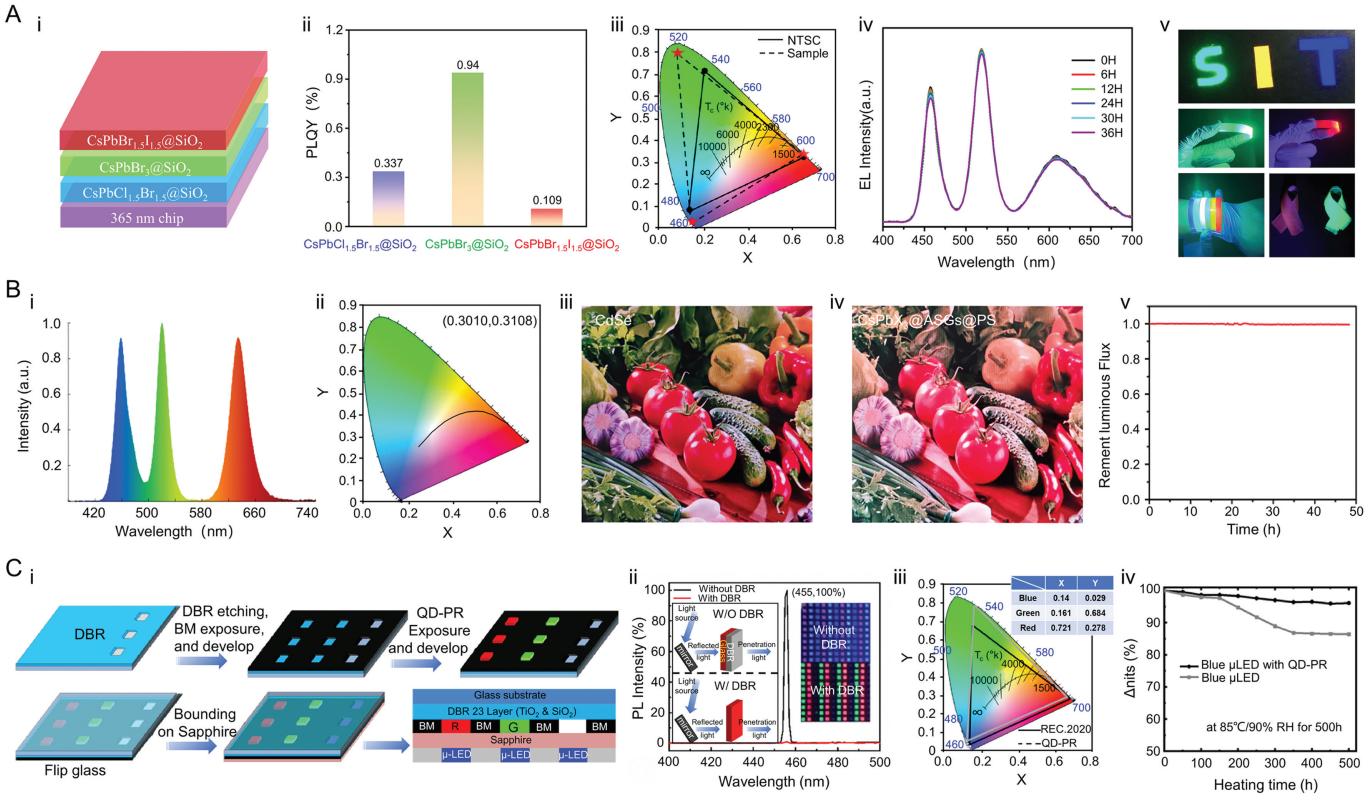

Fig. 6. Application of silica-coated QDs in color conversion-based LED devices. (A): (i) Structure of WLED; (ii) EL spectrum of the WLED device; (iii) The chromaticity diagram for the blue, green, and red $CsPbX_3@SiO_2$ NC films; (iv) Working stability of WLED devices; (v) The scalable and bendable light-emitting $CsPbX_3@SiO_2$ NC films were deposited on flexible substrates with a larger area or textile fibers. Reproduced with permission [64]. Copyright 2022, Elsevier. (B): (i) EL spectra of $CsPbX_3$@AGs@PS composite film; (ii) CIE chromaticity coordinates of the $CsPbX_3$@AGs@PS composites films prepared LED devices excited by blue backlight at 460 nm; (iii) Commercial CdSe composite film display images; (iv) $CsPbX_3$@AGs@PS composite film display images; (v) The stability of $CsPbX_3$@AG@PS was observed after 48 h of continuous backlight illumination. Reproduced with permission [65]. Copyright 2022, Elsevier. (C): (i) A schematic diagram of the deposition and patterning of the DBR layer; (ii) The PL intensity of the glass with and without the DBR layer; (iii) The micro-LED display's chromaticity diagram for the red, green, and blue QDPR pixels; (iv) The blue micro-LED display's brightness percentage trends over 500 h at 85 °C and 90% relative humidity with and without QD-PR pixels. Reproduced with permission [68]. Copyright 2022, Elsevier.

electrons and holes. Moreover, QLED employing A-$CsPbBr_3@SiO_2$ QDs demonstrated exceptional reliability, exhibiting a half-life of 43 min at 100 cd/m^2 under ambient conditions markedly better than the mere 2 min observed in QLED using original $CsPbBr_3$ QDs (Fig. 7A(v)). Furthermore, A-$CsPbBr_3@SiO_2$ QDs-based QLED maintained approximately 56% of their initial EL value after sustaining operation for 8 days at 3.2 V and approximately 20% humidity (Fig. 7A(vi)), validating the viability of employing silica-coated QDs as light emission layer in QLED devices.

However, low charge injection efficiency can limit the effectiveness of silica-coated QD-based QLEDs. Kim *et al.* addressed this by using a porous p-SiO_2 coating on $CsPbBr_3$ QDs ($CsPbBr_3$/p-SiO_2), improving charge injection and overall performance [72]. $CsPbBr_3$/p-SiO_2 composite films exhibited low leakage current densities and a high luminous efficiency of 42,314 cd/m² (Fig. 7B(i)). Compared with $CsPbBr_3$ QDs-based QLED devices, $CsPbBr_3$/p-SiO_2 based devices exhibit superior EQE and current efficiency, with EQE_{max} and CE_{max} values of 16.97% and 70.06 cd/A, respectively (Fig. 7B(ii)). The chrominance coordinates (x, y) on the CIE chrominance diagram for $CsPbBr_3$ and $CsPbBr_3$/p-SiO_2 based QLED devices (ranging from (0.1677, 0.7401) to (0.1676, 0.7447)) aligned with measured EL and PL spectra (Fig. 7B(iii, iv)). The mechanical strength and thermal stability of p-SiO_2 contributed to enhanced durability, giving $CsPbBr_3$/p-SiO_2 QLEDs about seven times the stability of $CsPbBr_3$ QD-based QLEDs, demonstrating the potential for high-performance QLEDs with this coating (Fig. 7B(v)). The overall device, showcasing these advancements, is visually represented in Fig. 7B(vi).

3.2. Solar cells

Solar cells, or photovoltaic cells, transform solar energy into electrical energy, significantly impacting daily life [73–75]. These cells use the photovoltaic effect in semiconductor materials, where photon energy excites electrons, generating electron-hole pairs. QDs innovate solar cell design by enhancing light absorption, improving charge transport, and increasing stability, thereby advancing efficiency and durability [76].

The high refractive index of silica enhances light capture in solar cells, boosting photoelectric conversion efficiency [77,78]. Rho *et al.* used silica-coated QD-embedded silica nanoparticles (SiO_2/QD/SiO_2) as a light-trapping layer in dye-sensitized solar cells (DSSC) [79]. While the unmodified DSSC showed a short-circuit current density (J_{SC}) of 7.38 mA/cm^2 and 3.92% efficiency, the SiO_2/QD/SiO_2 DSSC improved to 9.28 mA/cm^2 and 4.82% efficiency. The SiO_2/QD/SiO_2 DSSCs also demonstrated better incident photon-to-current efficiency (IPCE) across a wider wavelength range, confirming the effectiveness of the light-trapping layer. The stability of SiO_2/QD/SiO_2 DSSCs in iodide/triiodide-based electrolytes was validated over 168 h, highlighting the durability of the SiO_2 coating. Notably, SiO_2/QD/SiO_2 acts as a supplementary light-trapping layer, enhancing solar cell performance and stability without serving as a photosensitizer.

Silica-coated QDs also function as passivation layers, reducing charge recombination and improving stability and efficiency. Liu *et al.* explored ZnS/SiO_2 coatings as passivation layers for CdS/CdSe co-sensitized solar cells based on mixed metal oxides (MMOs) [80].

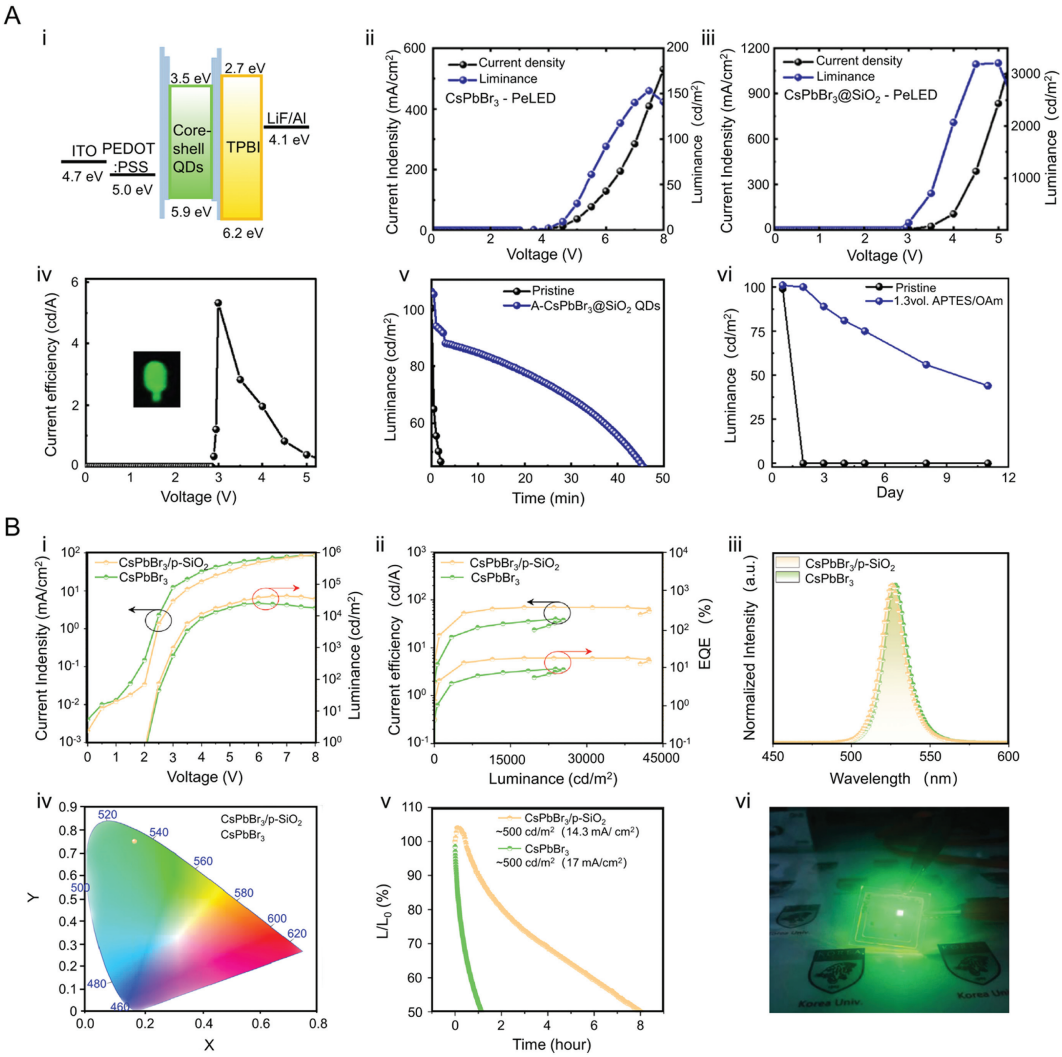

Fig. 7. Application of silica-coated QDs in EL-based LED. (A): (i) Device structure of QLED; Current density-voltage-brightness characteristics of QLED with (ii) $CsPbBr_3$ QLED and (iii) A-$CsPbBr_3$@SiO_2 QLED; (iv) Current efficiency-voltage characteristics of QLED; (v) Operational stability of QLED; (vi) Storage test of all-solution-processed QLED. Reproduced with permission [71]. Copyright 2021, American Chemical Society. (B): Current density-brightness-voltage (i), current efficiency-EQE-brightness (ii), EL spectrum (iii), CIE chromaticity diagram (iv), and lifetime (v) of $CsPbBr_3$ and $CsPbBr_3$/p-SiO_2 composite based QLED; (vi) A photograph of the $CsPbBr_3$/p-SiO_2 composite QLED. Reproduced with permission [72]. Copyright 2024, American Chemical Society.

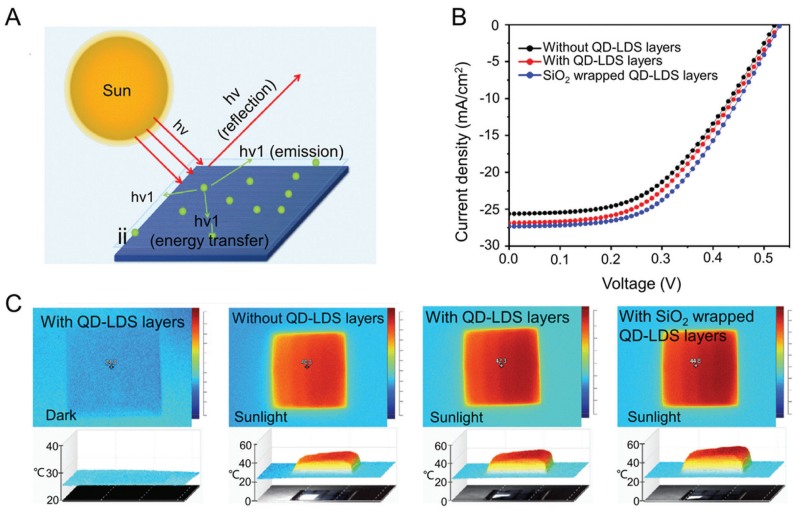

Fig. 8. Application of silica-coated QDs in solar cells. (A) Schematic diagram of the QD-LDS layer solar cells structure and working mechanism. (B) The *J-V* characteristics of solar cells without the QD-LDS layer and with a different QD-LDS layer in daylight. (C) Thermal imaging pictures of solar cells taken both in the dark and after 30 min in the sun. Reproduced with permission [81]. Copyright 2024, Elsevier.

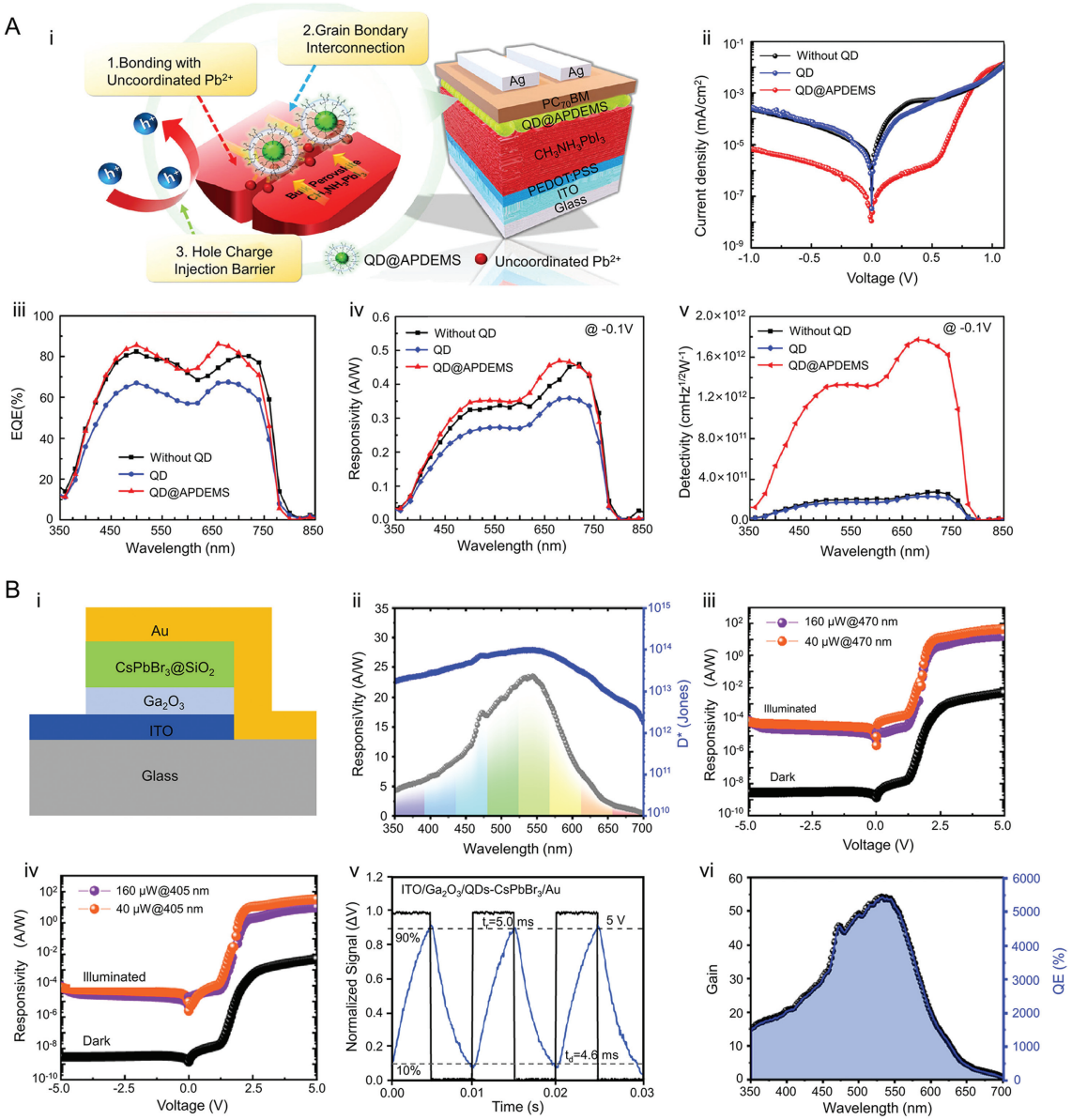

Fig. 9. Application of silica-coated QDs in photodetector. (A): (i) QD@APDEMS photodetector device structure; (ii) Dark *J-V* curves and (iii) EQE spectra of QD@APDEMS photodetector; (iv) QD@APDEMS photodetector device responsivity (at −0.1 V bias); (v) Detectivity of QD@APDEMS photodetector (at −0.1 V bias). Reproduced with permission [87]. Copyright 2023, John Wiley & Sons. (B): (i) Illustration of photodetector structure; Responsivity (ii), detectivity (iii), the rise/decay time (iv), and EQE (v) of photodetector. Reproduced with permission [89]. Copyright 2024, Royal Society of Chemistry.

Silica acts as an energy barrier, preventing electron migration to the electrolyte and suppressing recombination. Solar cells treated with ZnS/SiO_2 showed improved IPCE by 25% and 18% for ZnS/1h-SiO_2 and ZnS/2h-SiO_2 (where 1 h and 2 h represent the time of hydrolysis of silica), respectively. The ZnS/SiO_2 dual passivation layer further increased impedance, reducing charge recombination. Solar cells with ZnS/1h-SiO_2 achieved a power conversion efficiency (PCE) of 4.91%, a 36% improvement over single-layer passivation and 55% over unpassivated cells.

Silica-coated QDs can act as light-emitting downshifting (LDS) layers, converting high-energy photons into lower-energy ones that are more easily absorbed by solar cells. Zhao *et al.* integrated SiO_2-coated $Cs_3Bi_2Br_9$ QDs as an LDS layer in silicon solar cells (Fig. 8A) [81]. The $Cs_3Bi_2Br_9$ QDs efficiently converted ultraviolet photons to blue-region photon energy, reducing energy loss and increasing output. The silica shell facilitated chemical bonding with the silicon substrate, enhancing the connection between QDs and the photonic framework. The solar cell with the $Cs_3Bi_2Br_9$ QD LDS layer achieved a PCE of 15.24%, a J_{SC} of 26.87 mA/cm^2, and a V_{OC} of 0.52 V. With the $Cs_3Bi_2Br_9$@SiO_2-LDS layer, the cell improved to a PCE of 16.30%, J_{SC} of 27.33 mA/cm^2, and V_{OC} of 0.54 V, demonstrating a 1.82% increase in efficiency (Fig. 8B). The SiO_2 coating enhanced electron transfer and reduced nonradiative recombination by passivating interfacial defects (Fig. 8C).

3.3. Photodetectors

A photodetector is a device that can receive and detect optical radiation by converting light signals, such as ultraviolet, visible, and infrared light, into electrical signals. It is widely used in areas like optical detection [82,83], spectral analysis [84], and optical communication [85,86]. QDs are crucial in photodetectors, improving light absorption, carrier separation efficiency, response speed, and sensitivity. Researchers enhance spectral selectivity by

adjusting QD size and composition, allowing selective light detection. Silica-coated QDs act as a barrier layer, preventing hole carrier injection from the active region, thereby boosting detector performance and stability.

Chun *et al*. fabricated photodetector devices using QDs capped with 3-aminopropyl(diethoxy)methylsilane (QD@APDEMS) as hole carriers in the barrier layer (Fig. 9A(i)) [87]. The device current density of QD@APDEMS indicates that APDEMS significantly enhance photodetector performance and mitigate current leakage, improving signal-to-noise ratio and sensitivity (Fig. 9A(ii)). The QD@APDEMS-based photodetector showed a high EQE of 85% in the visible spectrum, converting light into current effectively (Fig. 9A(iii)). At a 0.1 V bias, response rates (R values) for QD@APDEMS, QD, and bare photodetectors are 0.469, 0.459, and 0.359 A/W, respectively (Fig. 9A(iv)). Detectivity (D^* values) for QD@APDEMS, QD, and bare devices are 1.77×10^{12}, 2.28×10^{11}, and 2.77×10^{11} cm $Hz^{-1/2}$ W^{-1}, respectively (Fig. 9A(v)), demonstrating superior performance of QD@APDEMS-based photodetectors.

Black *et al*. reported a unique heterostructured photodetector made of CdSe/ZnS QDs (CdSe/ZnS@SiO_2 QDs) covered in graphene and silica [88]. In these detectors, CdSe/ZnS@SiO_2 QDs enhance photoelectrical response performance through photosensitive defect states and semiconductor cores. The photogating effect captures light-excited holes while releasing electrons into graphene, achieving a charge carrier gain of up to 10^9, greatly improving sensitivity. Varying illumination power tunes graphene mobility, reducing from 1.14×10^{-1} m^2 V^{-1} s^{-1} to 4.5×10^{-2} m^2 V^{-1} s^{-1} due to Coulomb scattering. This demonstrates the potential of integrating CdSe/ZnS@SiO_2 QDs with graphene heterostructures for high-performance, tunable photodetectors.

Silica-coated QDs facilitate the creation of an integrated electric field between n-type and p-type layers, promoting carrier separation and enhancing detector response time and efficiency. Ely *et al*. developed a photodetector using $CsPbBr_3$@SiO_2 as the p-type layer, gallium oxide as the n-type layer, and Au as the hole collector (Fig. 9B(i)) [89]. The detector showed a high detection rate of over 9×10^{13} Jones across 350–640 nm (Fig. 9B(ii)). Under illumination at 160 μW and 40 μW, photocurrent increased by 4 orders of magnitude, reaching peaks of R values = 44.4 A/W and 32.0 A/W at +5 V for 470 nm and 405 nm, respectively (Fig. 9B(iii, iv)). It achieved a peak EQE of 5000%, a switching ratio of $\sim 10^4$, and rise/decay times of 5.0/4.6 ms (Fig. 9B(v, vi)). High-voltage bias enabled EQE > 100%, due to efficient charge injection and superior material quality.

4. Summary and outlook

This review explores the methodologies for fabricating silica-coated QDs and surveys advancements in their applications across diverse domains. To date, researchers have employed two principal coating techniques: hydrolysis and template method. The hydrolysis method, which includes the sol-gel and reverse microemulsion techniques, allows for precise control over the thickness and structure of the silica shell by adjusting precursor quantities and reaction times, ensuring uniform shell thickness and effective protection of the QDs. Template methods, which are further classified into low-temperature synthesis and high-temperature solid-phase techniques, utilize templates such as molecular sieves and microspheres to guide the growth and coating of QDs. The distinctive physicochemical attributes of QD@SiO_2 materials endow them with broad application prospects in the realms of optoelectronics. In the domain of optoelectronics, their integration into LED, solar cells and photodetectors are recognized for their superior photoelectric conversion efficiency coupled with enhanced stability.

Though ambient progresses, silica coating techniques still require enhancements to further improve the performance of QDs. The hydrolysis method for preparing silica coatings necessitates a prolonged reaction time and is easily affected by environmental factors like humidity and temperature. Consequently, precise control of reaction conditions is essential for achieving more uniform coating speed. The template method yields silica-coated QDs with large dimensions (typically exceeding 200 nm), necessitating size reduction for applications such as high-resolution micro-displays. A feasible strategy might involve reducing the size of large silica-coated QDs through mechanical grinding methods and effectively screening for well-coated QDs. Efficient surface modifications on silica coatings are often employed in most optoelectronic applications, such as the modification of high-conductance molecules to enhance charge transport efficiency. This requires high uniform and dense silica coatings on QDs, a challenge that can be addressed through more controllable coating processes and the adoption of multiple coating layers.

Declaration of competing interest

The authors declare that they have no known competing financial interests or personal relationships that could have appeared to influence the work reported in this paper.

CRediT authorship contribution statement

Siting Cai: Writing – original draft. **Xiang Chen:** Writing – original draft. **Shuli Wang:** Writing – review & editing, Project administration. **Xinqin Liao:** Writing – review & editing. **Zhong Chen:** Project administration. **Yue Lin:** Writing – review & editing, Project administration.

Acknowledgments

This work is supported by the National Natural Science Foundation of China (Nos. 62374142 and 22005255), Fundamental Research Funds for the Central Universities (Nos. 20720220085 and 20720240064), External Cooperation Program of Fujian (No. 2022I0004), Major Science and Technology Project of Xiamen in China (No. 3502Z20191015), Xiamen Natural Science Foundation Youth Project (No. 3502Z202471002).

References

[1] T. Qiao, D.H. Son, Acc. Chem. Res. 54 (2021) 1399–1408.
[2] X. Luo, R. Lai, Y. Li, et al., J. Am. Chem. Soc. 141 (2019) 4186–4190.
[3] T. VanWie, E. Wysocki, J.R. McBride, et al., Chem. Mater. 31 (2019) 8558–8562.
[4] A. Ashokan, J.A. Hutchison, P. Mulvaney, Chem. Mater. 36 (2024) 1810–1817.
[5] S. Liu, K. Xiong, K. Wang, et al., ACS Nano 15 (2021) 3376–3386.
[6] H. Wang, J. Pinna, D.G. Romero, et al., Adv. Mater. 36 (2024) 2311526.
[7] B. Chen, D. Li, F. Wang, Small 16 (2020) 2002454.
[8] H.B. Jalali, L.D. Trizio, L. Manna, et al., Chem. Soc. Rev. 51 (2022) 9861–9881.
[9] P. Ding, P. Ko, P. Geng, et al., Adv. Opt. Mater. 12 (2024) 2302477.
[10] Y. Han, X. Chang, X. Cheng, et al., Laser Photonics Rev. 17 (2023) 2300383.
[11] Q. Zeng, X. Zhang, X. Feng, et al., Adv. Mater. 30 (2018) 1705393.
[12] R. Zhou, J. Xu, P. Luo, et al., Adv. Energy Mater. 11 (2021) 2101923.
[13] D. Kim, G. Cho, Y.H. Kim, et al., Adv. Energy Mater. 14 (2024) 2302579.
[14] L. Kong, X. Zhang, C. Zhang, et al., Adv. Mater. 34 (2022) 2205217.
[15] W. Yan, J. Shen, Y. Zhu, et al., Nano Res. 14 (2021) 4038–4045.
[16] K. Shibata, M. Yoshida, K. Hirakawa, et al., Nat. Commun. 14 (2023) 7486.
[17] J. Wen, H. Hu, G. Wen, et al., J. Phys. D: Appl. Phys. 54 (2021) 114002.
[18] J. Zhou, R. Zhao, Y. Du, et al., Adv. Funct. Mater. 32 (2022) 2112083.
[19] B. Huang, T. Tang, F. Liu, et al., Chin. Chem. Lett. 35 (2024) 109694.
[20] W. Su, R. Guo, F. Yuan, et al., J. Phys. Chem. Lett. 11 (2020) 1357–1363.
[21] M. Díaz-González, A. Escosura-Muñiz, M.T. Fernandez-Argüelles, Top. Curr. Chem. 378 (2020) 133–176.
[22] P. Zhu, Y. Liu, Y. Tang, et al., Chin. Chem. Lett. 35 (2024) 108689.
[23] R. Cheng, Z.B. Liang, H. Shen, et al., Chin. Chem. Lett. 34 (2023) 107384.
[24] P. He, W. Ge, Q. Zhang, et al., Ceram. Int. 50 (2024) 20285–20292.
[25] S. Ding, J.A. Steele, P. Chen, et al., Adv. Energy Mater. 13 (2023) 2301817.
[26] Q. Zeng, X. Zhang, Q. Bing, et al., ACS Energy Lett. 7 (2022) 1963–1970.
[27] Z. Qi, X. Mei, J. Wang, et al., Adv. Funct. Mater. 34 (2024) 2405679.
[28] J.I. Kim, Q. Zeng, S. Park, et al., Adv. Mater. 35 (2023) 2209784.
[29] Q. Huang, W. Yin, B. Gao, et al., Light: Sci. Appl. 13 (2024) 111.

[30] J. Cai, W. Lai, Y. Chen, et al., Laser Photonics Rev. 18 (2024) 2400298.
[31] X. Yang, S. Wang, Y. Hou, et al., Nano Lett. 24 (2024) 3661–3669.
[32] Y. Chen, X. Yang, X. Fan, et al., ACS Appl. Mater. Interfaces 16 (2024) 24908–24919.
[33] Y. Jung, Y.S. Shim, Y.K. Kim, J. Mater. Sci. 56 (2021) 12315–12325.
[34] Y. Yu, J. Guo, F. Bian, et al., Sci. China Mater. 64 (2021) 2858.
[35] S. Ma, J. Li, Z. Liu, Chem. Phys. Lett. 843 (2024) 141242.
[36] X. He, D. Sui, Chem. Pap. 77 (2023) 5807–5815.
[37] J.C. Echeverría, P. Moriones, G. Arzamendi, et al., J. Sol-Gel Sci. Techn. 86 (2018) 316–328.
[38] S. Sakka, J. Sol-Gel Sci. Technol. 102 (2022) 478–481.
[39] C. Liu, W. Huang, J. Li, et al., Adv. Opt. Mater. 11 (2023) 2300963.
[40] L. Ding, Y. Chen, Z. Hua, et al., New J. Chem. 44 (2020) 2122–2128.
[41] Q. Zhong, M. Cao, H. Hu, et al., ACS Nano 12 (2018) 8579–8587.
[42] C. Meng, D. Yang, Y. Wu, et al., J. Mater. Chem. C 8 (2020) 17403–17409.
[43] L. Chao, J. Tang, S. Lin, et al., Mater. Sci. Semicond. Process. 136 (2021) 106158.
[44] X. Fan, S. Wang, X. Yang, et al., Adv. Mater. 35 (2023) 2300834.
[45] J. Xue, H. Li, J. Liu, et al., Mater. Lett. 242 (2019) 143–146.
[46] R. An, H. Gao, S. Shi, et al., IEEE Trans. Electron Devices 69 (2022) 575–581.
[47] Y. Lv, J. Li, R. Wu, et al., Biochem. Eng. J. 137 (2018) 344–351.
[48] X. Tang, W. Chen, Z. Liu, et al., Small 15 (2019) 1900484.
[49] X. Huang, X. Zeng, J. Wang, et al., J. Mater. Sci. 54 (2019) 8581–8590.
[50] H. Yoo, K. Woo, J. Phys. Chem. Lett. 9 (2018) 2106–2112.
[51] M. Fan, J. Huang, L. Turyanska, et al., Adv. Funct. Mater. 33 (2023) 2215032.
[52] F.Lin Huang, F. Li, et al., Angew. Chem. 136 (2024) e202402520.
[53] P. Chen, Y. Liu, Z. Zhang, et al., Nanoscale 11 (2019) 16499–16507.
[54] Q. Zhang, B. Wang, W. Zheng, et al., Nat. Commun. 11 (2020) 31.
[55] Y. Lin, X. Fan, X. Yang, et al., Small 17 (2021) 2103510.
[56] Y. Lin, X. Zheng, Z. Shangguan, et al., J. Mater. Chem. C 9 (2021) 12303–12313.
[57] T. Yang, Y. Zhu, X. Yang, et al., Adv. Mater. Interfaces 9 (2022) 2200571.
[58] M. He, Q. Zhang, F. Carulli, et al., ACS Energy Lett. 8 (2023) 151–158.
[59] W. Song, L. Liu, W. Zhou, et al., ACS Appl. Nano Mater. 5 (2022) 11549–11558.
[60] R. Deng, X. Fan, G. Chen, et al., J. Lumin. 257 (2023) 119701.
[61] E. Jang, H. Jang, Chem. Rev. 123 (2023) 4663.
[62] A. Fakharuddin, M.K. Gangishetty, M. Abdi-Jalebi, et al., Nat. Electron. 5 (2022) 203–216.
[63] X. Yang, Y. Lin, T. Wu, et al., Opto-Electron. Adv. 5 (2022) 210123 -1.
[64] C. Wang, C. Zhang, F. Wang, et al., J. Alloys Compd. 925 (2022) 166551.
[65] Z. Chen, J. Zhao, R. Zeng, et al., Chem. Eng. J. 433 (2022) 133195.
[66] X. Kong, X. Fan, Y. Wang, et al., Nano Mater. Sci. 7 (2025) 49–64.
[67] X. Fan, X. Yang, X. Kong, et al., Next Nanotech. 5 (2024) 100045.
[68] K. Chang, C. Wu, C. Lo, et al., Mater. Sci. Semicond. Process. 148 (2022) 106790.
[69] Q. Chen, Y. Hu, J. Lin, et al., Nanoscale Horiz. 9 (2024) 465–471.
[70] Y. Nong, J. Yao, J. Li, et al., Adv. Mater. (2024) 2402325.
[71] C.K. Trinh, H. Lee, M.G. So, et al., ACS Appl. Mater. Interfaces 13 (2021) 29798–29808.
[72] B.W. Kim, H. Noh, K.H. Kim, et al., Adv. Mater. Interfaces 11 (2024) 2400116.
[73] S. Ramakrishnan, D. Song, Y. Xu, et al., Adv. Energy Mater. 13 (2023) 2302240.
[74] T. Zhu, Y. Yang, S. Zhou, et al., Chin. Chem. Lett. 31 (2020) 2249–2253.
[75] X. Yang, J. Han, W. Ruan, et al., Chin. Chem. Lett. 33 (2022) 1425–1429.
[76] Y. Zhang, Z. Liu, W. Ma, J. Phys. Chem. Lett. 14 (2023) 6402–6413.
[77] J. Wang, H. Zhang, L. Wang, ACS Appl. Energy Mater. 3 (2020) 4484–4491.
[78] P. Ye, J. Peng, F. Xu, et al., Prog. Org. Coat. 184 (2023) 107827.
[79] W.Y. Rho, J.W. Choi, H.Y. Lee, et al., New J. Chem. 38 (2014) 910–913.
[80] J. Liu, J. Liu, C. Wang, et al., Sol. Energy Mater. Sol. Cells 208 (2020) 110380.
[81] X. Zhao, X. Zhang, X. Liu, et al., Colloids Surf. A 682 (2024) 132887.
[82] Z. Lin, Z. Wang, N. Zhang, et al., Nano Today 56 (2024) 102281.
[83] C. Tan, R. Tao, Z. Yang, et al., Chin. Chem. Lett. 34 (2023) 107979.
[84] D. Shen, H. Yang, C. Spudat, et al., Nano Lett. 22 (2022) 3425–3432.
[85] Z. Wang, Y. Gao, Y. Li, et al., Adv. Funct. Mater. 34 (2024) 2310911.
[86] Y. Chai, J. Jiang, L. Wu, et al., J. Phys. Chem. Lett. 15 (2024) 3859–3865.
[87] J.Y. Chun, B.G. Kim, J.Y. Kim, et al., Carbon Energy 5 (2023) e350.
[88] A. Black, F.J. Urbanos, J. Roberts, et al., ACS Omega 4 (2019) 15824–15828.
[89] F. Ely, K.O. Vieira, M.G. Reyes-Banda, et al., Nanoscale 16 (2024) 10833–10840.